DIFFERENTIAL FEEDBACK IN MIMO COMMUNICATIONS: PERFORMANCE WITH DELAY AND REAL CHANNEL MEASUREMENTS

Daniel Sacristán-Murga[1], *Florian Kaltenberger*[2], *Antonio Pascual-Iserte*[1,3], *Ana I. Pérez-Neira*[1,3]

[1]Centre Tecnològic de Telecomunicacions de Catalunya (CTTC) - Spain
[2]Mobile Communications - Institut Eurecom - France
[3]Dept. of Signal Theory and Communications - Universitat Politècnica de Catalunya (UPC) - Spain
email: daniel.sacristan@cttc.es, florian.kaltenberger@eurecom.fr, antonio.pascual@upc.edu, ana.isabel.perez@upc.edu

ABSTRACT

This work studies the performance of our recently proposed differential feedback scheme for multi-input-multi-output (MIMO) communication systems using real channel measurement data. The algorithm is applied to the channel correlation matrix exploiting geodesic curves and the intrinsic geometry of positive definite Hermitian matrices. The performance of this and a conventional non-differential feedback scheme are evaluated using real data and channel measurements obtained with the Eurecom MIMO OpenAir Sounder (EMOS). Additionally, the impact of having a delay in the feedback link is also studied in terms of a loss of performance in the communication through several simulations.

The results show that the differential feedback strategy performs much better than the non-differential strategies in low mobility channels, while in high mobility channels the performance is similar. A delay in the feedback channel affects specially high mobility channels while having a negligible impact in the slow-varying cases.

Topics: Precoding and limited feedback, Multi-antenna channel measurements, MIMO systems.

1. INTRODUCTION

Multi-input-multi-output (MIMO) communication systems are shown to provide improved performance when compared to single-antenna configurations, specially when both the transmitter and the receiver have some kind of channel state information (CSI). A possibility to obtain CSI at the transmitter consists in the exploitation of a low rate feedback channel from the receiver to the transmitter. A feedback channel is mandatory in frequency-division duplexing channels, where channel reciprocity does not hold.

In the literature, several feedback schemes have been proposed in order to provide CSI to the transmitter side. For time-varying channels, where the coherence time is higher than the time difference between consecutive feedback instants, a good approach consists in quantizing the channel response in a differential way. This lowers the required feedback load or improves the quality of the quantization for a fixed capacity of the feedback link. Taking this philosophy, there are several techniques, such as the direct scalar quantization of the entries of the channel variation matrix, or more sophisticated approaches, such as those based on geodesic curves over Grassmannian manifolds or correlation-type matrices [1–3].

All these real time feedback schemes suffer from the delay inherent to the feedback channel. This delay causes a mismatch between the true channel and the available CSI and, consequently, between the actual design of the transmitter and the optimum one, which results in a degradation of the performance. The effect of the delay can be alleviated using a channel predictor.

The main objective of this paper is to evaluate experimentally in a real environment the performance of different feedback strategies and the impact of feedback delay. This will be done taking as example the differential technique presented in [3] for feedback and channel quantization (this technique will be summarized in the subsequent sections) and a non-differential feedback strategy from [4]. Both of them will be applied to real channel measurements obtained with the Eurecom's MIMO OpenAir Sounder (EMOS) [5, 6]. In order to alleviate the effect of feedback delay a technique based on channel prediction will be studied. In particular a linear Wiener predictor will be considered.

The paper is organized as follows. The system and signal models are given in section 2. Section 3 summarizes the differential quantization technique used in the feedback link, and section 4 describes the EMOS and the channel measurements. The performance of differential versus non-differential feedback strategies applied to the measured channel, including an analysis of the effect of feedback delay, is shown in section 5. A solution based on prediction is presented in 6. Finally, section 7 concludes the paper.

This work was partially supported by the Catalan Government under grant 2005SGR-00996; by the Spanish Government under projects TEC2008-06327-C03-01 (FBMC-MULAN) and 2A103 (MIMOWA) from MEDEA+ program (AVANZA I+D TSI-020400-2008-150), by the European Commission under projects NEWCOM++ (216715) and CHORIST; and by Eurecom.

2. SYSTEM AND SIGNAL MODELS

This section and the next one summarize some of the ideas presented in [3] concerning the differential feedback technique that will be used in this paper to evaluate a realistic system performance according to real channel measurements.

We consider the transmission through a MIMO channel with n_T and n_R transmit and receive antennas represented at time instant n by matrix $\mathbf{H}(n) \in \mathbb{C}^{n_R \times n_T}$. The n_R received signals at the same time instant, assuming a linear transmitter, can be expressed as

$$\mathbf{y}(n) = \mathbf{H}(n)\mathbf{B}\big(\widehat{\mathbf{R}}_H(n)\big)\mathbf{x}(n) + \mathbf{w}(n) \in \mathbb{C}^{n_R}, \quad (1)$$

where $\mathbf{x}(n) \in \mathbb{C}^{n_S}$ represents the n_S streams of signals to be transmitted with $\mathbb{E}\big[\mathbf{x}(n)\mathbf{x}^H(n)\big] = \mathbf{I}$, and $\mathbf{B} \in \mathbb{C}^{n_T \times n_S}$ is the linear transmitter matrix. Note that we explicitly indicate that the transmitter depends on the available estimate of the channel correlation matrix $\widehat{\mathbf{R}}_H(n)$, where the exact channel correlation matrix is $\mathbf{R}_H(n) = \mathbf{H}^H(n)\mathbf{H}(n)$. The additive white Gaussian noise (AWGN) at the receiver is represented by $\mathbf{w}(n) \in \mathbb{C}^{n_R}$ with $\mathbb{E}\big[\mathbf{w}(n)\mathbf{w}^H(n)\big] = \sigma_w^2\mathbf{I}$.

In the system setup, it will be considered that the receiver knows perfectly the current channel matrix $\mathbf{H}(n)$ and that the transmitter designs $\mathbf{B}$ assuming that the available CSI at its side represented by $\widehat{\mathbf{R}}_H(n)$ is also perfect. In reality, the CSI at the transmitter is not perfect because it is a quantized version of the perfect CSI obtained at the receiver. The transmitter design can be done according to different criteria, such as the maximization of the mutual information or signal to noise ratio (SNR), or the minimization of the mean square error (MSE) or the bit error rate (BER), among others. In all the cases, the optimum transmitter has been shown to depend only on the channel correlation matrix $\mathbf{R}_H(n)$ [7]. For each of them a cost function $d(\widehat{\mathbf{R}}_H(n), \mathbf{H}(n))$ can be defined, where the design objective is its minimization. A couple of examples of cost functions are given in the following paragraphs, although any criterion can be applied (we drop the dependency with respect to the time index n for the sake of clarity in the notation).

The cost function that follows a maximum SRN with single beamforming (number of streams $n_S = 1$) criteria can be expressed as

$$d(\widehat{\mathbf{R}}_H(n), \mathbf{H}(n)) = -\frac{1}{\sigma_w^2}\left\|\mathbf{H}\mathbf{B}\right\|_F^2, \quad (2)$$

where the transmission matrix $\mathbf{B} \in \mathbb{C}^{n_T \times 1}$ is defined as

$$\mathbf{B}\big(\widehat{\mathbf{R}}_H(n)\big) = \sqrt{P_T}\,\mathbf{u}_{\max}\big(\widehat{\mathbf{R}}_H(n)\big), \quad (3)$$

and $\mathbf{u}_{\max}(\cdot)$ stands for the unit-norm eigenvector of maximum associated eigenvalue. P_T represents the maximum transmission power, i.e., $\|\mathbf{B}\|_F^2 \leq P_T$, where subindex F stands for the Frobenius norm.

The cost function that maximizes the mutual information can be expressed as

$$d(\widehat{\mathbf{R}}_H(n), \mathbf{H}(n)) = -\log_2\left|\mathbf{I} + \frac{1}{\sigma_w^2}\mathbf{B}\mathbf{B}^H\mathbf{H}^H\mathbf{H}\right|, \quad (4)$$

where the transmission matrix $\mathbf{B} \in \mathbb{C}^{n_T \times n_S}$ is defined as

$$\mathbf{B}\big(\widehat{\mathbf{R}}_H(n)\big) = \widetilde{\mathbf{U}}(n)\mathbf{P}^{1/2}(n), \quad (5)$$

$$\mathbf{P}(n) = \mathrm{diag}(p_1, \ldots, p_{n_S}), \quad (6)$$

and $\widetilde{\mathbf{U}}(n)$ consists of n_S columns that are the n_S unit-norm eigenvectors of $\widehat{\mathbf{R}}_H(n)$ associated to its n_S maximum eigenvalues $\{\lambda_i\}_{i=1}^{n_S}$. The power $\mathbf{P}(n)$ is allocated according to the waterfilling solution ($p_i = \max\{0, \mu - 1/\lambda_i\}$ where μ is a constant such that $\sum_{i=1}^{n_S} p_i = P_T$) [7].

The next section is devoted to summarize algorithm [3] for quantizing the actual correlation matrix $\mathbf{R}_H$ (instead of $\mathbf{H}$) from the receiver to the transmitter in a differential way. Since $\mathbf{R}_H$ belongs to the set of Hermitian positive definite matrices,[1] exploiting its inherent geometry will improve the performance of the quantization.

3. ALGORITHM DESCRIPTION FOR QUANTIZATION IN FEEDBACK LINK

In this section first we will give some comments on the concept of geodesic curves on the set of positive definite Hermitian matrices and then we will summarize the basic ideas concerning the algorithm presented in [3] for differential quantization.

3.1. Geodesic curves

As shown in [2] the set of Hermitian positive definite matrices $\mathcal{S} = \{\mathbf{R} \in \mathbb{C}^{n_T \times n_T} : \mathbf{R}^H = \mathbf{R}, \mathbf{R} \succ \mathbf{0}\}$ is a convex cone[2], i.e., $\forall \mathbf{R}_1, \mathbf{R}_2 \in \mathcal{S}, \forall s \geq 0,\ \mathbf{R}_1 + s\mathbf{R}_2 \in \mathcal{S}$ [8]. This set is characterized properly by means of differential geometry, which states a set of definitions for the distance, scalar products and routes within this set:

- *Scalar product:* At any point in this set $\mathcal{S}$ given by $\mathbf{R}$ (also named as *base point*), the scalar product between two Hermitian matrices $\mathbf{A}$ and $\mathbf{B}$ is defined as $\langle \mathbf{A}, \mathbf{B}\rangle_{\mathbf{R}} = \mathrm{Tr}(\mathbf{R}^{-1}\mathbf{A}\mathbf{R}^{-1}\mathbf{B})$. This definition implies that the norm is defined as $\|\mathbf{A}\|_{\mathbf{R}} = \sqrt{\mathrm{Tr}(\mathbf{R}^{-1}\mathbf{A}\mathbf{R}^{-1}\mathbf{A})}$.

[1] In the following, it will be assumed that the channel correlation matrix is strictly positive definite. If this cannot be guaranteed because, for example, if $n_R < n_T$, it is possible to work with extended correlation matrices defined as $\widetilde{\mathbf{R}}_H = \mathbf{H}^H\mathbf{H} + \epsilon\mathbf{I},\ \epsilon > 0$, which are positive definite by construction.

[2] Actually, reference [2] is devoted to the case of real matrices, although the results and conclusions can be extended directly to the complex case.

- *Geodesic curve:* Given two points $\mathbf{R}_1$and $\mathbf{R}_2$ in the set $\mathcal{S}$, the geodesic curve, which is the curve connecting these points with minimum distance and with all its points belonging to $\mathcal{S}$, is given by

$$\Gamma(t) = \mathbf{R}_1^{1/2} \exp\left(t\mathbf{C}\right)\mathbf{R}_1^{1/2}, \tag{7}$$

  where $\mathbf{C} = \log\left(\mathbf{R}_1^{-1/2}\mathbf{R}_2\mathbf{R}_1^{-1/2}\right)$, $\Gamma(0) = \mathbf{R}_1$, and $\Gamma(1) = \mathbf{R}_2$. The derivative of the geodesic curve at $t = 0$, which is in fact the *direction* of such curve at $t = 0$, is given by the Hermitian matrix $\Gamma'(0) = \mathbf{R}_1^{1/2}\mathbf{C}\mathbf{R}_1^{1/2}$.

- *Distance:* The geodesic distance between any two points in $\mathcal{S}$ is given by the length of the geodesic curve that connects them. According to the previous notation, it can be shown that this distance is given by

$$d_g(\Gamma(0),\Gamma(t)) = |t|\|\mathbf{C}\|_F, \;\Rightarrow\; d_g(\mathbf{R}_1,\mathbf{R}_2) = \|\mathbf{C}\|_F. \tag{8}$$

  or, using an equivalent expression,

$$d_g(\mathbf{R}_1,\mathbf{R}_2) = \Big(\sum_i |\log\lambda_i|^2\Big)^{1/2}, \tag{9}$$

  where $\{\lambda_i\}$ are the eigenvalues of matrix $\mathbf{R}_1^{-1/2}\mathbf{R}_2\mathbf{R}_1^{-1/2}$.

3.2. Differential quantization

In general terms, differential quantization is based on a quantization of the difference between the CSI at consecutive feedback intervals, instead of quantizing the complete CSI every time [4]. Depending on the design criterion and the allowed computational complexity, different strategies arise.

Some techniques can be based on the quantization of the variations of the MIMO channel matrix $\mathbf{H}(n)$ itself or even, on the differential quantization of the strongest right eigenspaces spanned by such matrices [1]. The technique that will used in this paper to evaluate experimentally the performance of the communication setup corresponds to reference [3]. It relies on the fact that in general, all the joint transmitter-receiver designs for MIMO channels and different quality criteria (SNR, MSE, mutual information, etc.) depend on the channel response matrix $\mathbf{H}(n)$ only through the channel correlation matrix defined as $\mathbf{R}_H(n) = \mathbf{H}^H(n)\mathbf{H}(n)$ [7]. Taking this into account, a possible strategy consists in applying a differential quantization exploiting the intrinsic geometry of the set of positive definite Hermitian matrices by means of the use of geodesic curves, as suggested in [2].

The fundamentals of the algorithm proposed in [3], which are summarized here, are based on a differential quantization of the channel correlation matrix $\mathbf{R}_H(n)$. The objective is to minimize the cost function as presented in section 2, which can be related to the quality measure of the system and, therefore, the receiver has to know which kind of design will be applied by the transmitter. If a more general setup is to be applied so that the feedback can be used for any transmitter design, another cost function could be added which is simply the geodesic distance between the actual channel correlation matrix and its fed back estimate, i.e., $d(\widehat{\mathbf{R}}_H(n), \mathbf{H}(n)) = d_g(\widehat{\mathbf{R}}_H(n), \mathbf{H}^H(n)\mathbf{H}(n))$.

The differential quantization algorithm for the feedback of the channel correlation matrix is an iterative procedure. At each iteration n the initial situation is described as follows: the receiver has a perfect knowledge of the current channel matrix $\mathbf{H}(n)$ and both the transmitter and the receiver know which is the last estimate of the channel correlation matrix sent through the feedback channel $\widehat{\mathbf{R}}_H(n-1)$. A possible initialization of the algorithm would correspond to starting the run of the algorithm from the cone vertex before the first iteration: $\widehat{\mathbf{R}}_H(0) = \mathbf{I}$.

At each iteration n, the following steps are followed (all these steps are represented conceptually in Fig. 1):

- *STEP 1:* Both the receiver and the transmitter generate a common set of Q random Hermitian matrices using the same pseudo-random generator and the same seed. Then, these matrices are orthonormalized using the Gram-Schmidt procedure [9] according to the definition of scalar product presented in section 3, producing the set $\{\mathbf{A}_i\}_{i=1}^{Q}$. Finally, each matrix $\mathbf{A}_i$ is rescaled individually so that $\mathbf{C}_i = \mathbf{R}^{-1/2}\mathbf{A}_i\mathbf{R}^{-1/2}$ has a norm equal to Δ ($\|\mathbf{C}_i\|_F = \Delta$) which is, in fact, the quantization step.

- *STEP 2:* Both the receiver and the transmitter use the previous matrices to generate a set of Q geodesic curves $\{\Gamma_i(t)\}_{i=1}^{Q}$, all of them having the same initial point $\mathbf{R} = \widehat{\mathbf{R}}_H(n-1)$ and with orthogonal directions: $\Gamma_i(t) = \widehat{\mathbf{R}}_H^{1/2}(n-1)\exp\left(t\mathbf{C}_i\right)\widehat{\mathbf{R}}_H^{1/2}(n-1)$.

- *STEP 3:* Each of these geodesic curves is used to generate two candidates for the feedback in the next iteration $\widehat{\mathbf{R}}_H(n)$ corresponding to $\Gamma_i(-1)$ and $\Gamma_i(1)$.

- *STEP 4:* The receiver evaluates the cost function for each of the candidates (there are $2Q$ candidates), and sends the selected index i_{FB} through the feedback channel to the transmitter. This index is the one for which the corresponding candidate minimizes the cost function. According to this, the number of feedback bits per iteration has to be higher than or equal to $\log_2(2Q)$. The matrix corresponding to the selected candidate will be used for the transmitter design and as the starting point in the next iteration.

All the previous steps are represented graphically in Fig. 1 for the case of a feedback using 2 bits and taking as optimization criterion the minimization of the geodesic distance to the actual channel correlation matrix $\mathbf{R}_H(n)$. Starting from $\widehat{\mathbf{R}}_H(n-1)$, the algorithm generates 2 orthogonal geodesic

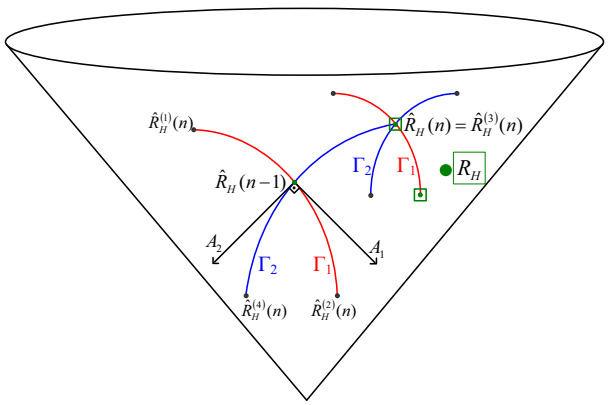

Fig. 1. 2-bit differential quantization in the space of channel correlation matrices.

routes $\Gamma_1(t)$ and $\Gamma_2(t)$ with velocity matrices $\mathbf{A}_1$ and $\mathbf{A}_2$, producing four quantization candidates, all of them at distance Δ from the initial point. At the receiver, each candidate is compared to the actual $\mathbf{R}_H$ and the one with smallest distance (in this example candidate 3) is chosen. That is, its index $i_{FB} = 3$ is sent to the transmitter through the feedback channel and $\widehat{\mathbf{R}}_H(n) = \widehat{\mathbf{R}}_H^{(3)}(n)$. The next iteration starts from this point, generates 2 orthogonal routes and 4 quantization candidates, selects the closest candidate to $\mathbf{R}_H$, and so on.

4. REAL CHANNEL MEASUREMENTS

Realistic MIMO channel measurements have been obtained using Eurecom's MIMO Openair Sounder (EMOS) [5, 6]. In this section we first describe the hardware of the EMOS platform and the channel sounding procedure and then the measurement campaign that was carried out for this paper. The obtained measurements are used in the next section to evaluate the previous feedback quantization technique from a realistic point of view.

4.1. Platform description

The EMOS is based on the OpenAirInterface hardware/software development platform at Eurecom.[3] It operates at 1.900-1.920 GHz with 5 MHz channels and can perform real-time channel measurements between a base station and multiple users synchronously. For the base station (BS), a workstation with four PLATON data acquisition cards (see Fig. 2(a)) is employed along with a Powerwave 3G broadband antenna (part no. 7760.00) composed of four elements which are arranged in two cross-polarized pairs (see Fig. 2(b)). The user equipment (UE) consists of a laptop computer with Eurecom's dual-RF CardBus/PCMCIA data acquisition card

[3] http://www.openairinterface.org

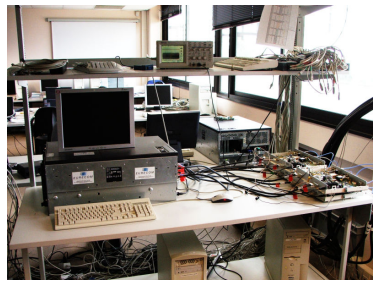

(a) Server PC with PLATON boards

(b) Powerwave Antenna

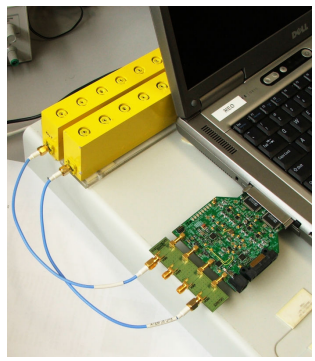

(c) Dual-RF CardBus/PCMCIA Card

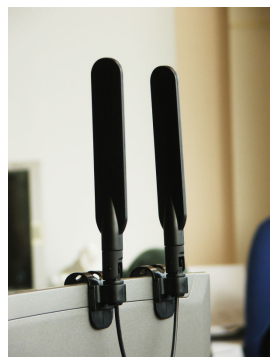

(d) Panorama Antennas

Fig. 2. EMOS base-station and user equipment [10].

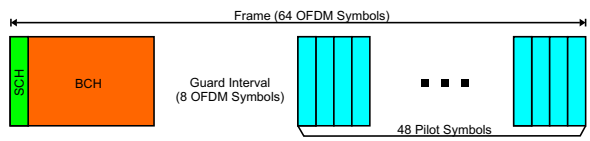

Fig. 3. Frame structure of the OFDM Sounding Sequence. The frame consists of a synchronization channel (SCH), a broadcast channel (BCH), and several pilot symbols used for channel estimation.

(see Fig. 2(c)) and two clip-on 3G Panorama Antennas (part no. TCLIP-DE3G, see Fig. 2(d)). The platform is designed for a full software-radio implementation, in the sense that all protocol layers run on the host PCs under the control of a Linux real time operation system.

Sounding Signal. The EMOS uses an OFDM modulated sounding sequence with 256 subcarriers (out of which 160 are non-zero) and a cyclic prefix length of 64. One transmit frame is 64 OFDM symbols (2.667 ms) long and consists of a synchronization symbol (SCH), a broadcast data channel (BCH) comprising 7 OFDM symbols, a guard interval, and 48 pilot symbols used for channel estimation (see Fig. 3). The pilot symbols are taken from a pseudo-random QPSK sequence defined in the frequency domain. The subcarriers of the pilot symbols are multiplexed over the transmit antennas to ensure orthogonality in the spatial domain. We can therefore obtain

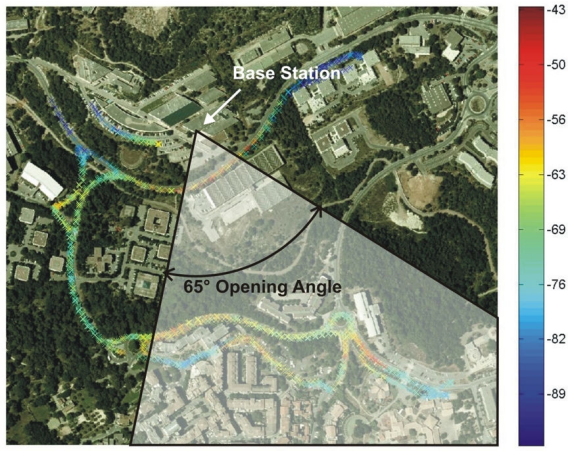

Fig. 4. Map of the measurement scenario. The position and the opening angle of the BS antenna are also indicated. The users were driving in cars along the indicated routes (the colors show the received signal strength in dBm along the routes).

Parameter	Value
Center Frequency	1917.6 MHz
Bandwidth	4.8 MHz
BS Transmit Power	30 dBm
Number of Antennas at BS	4 (2 cross polarized)
Number of UE	1
Number of Antennas at UE	2

Table 1. EMOS parameters.

one full MIMO channel estimate for one group of a number of subcarriers equal to the number of transmitter antennas. The BCH contains the frame number of the transmitted frame that is used for synchronization among the UEs.

Channel Estimation Procedure. Each UE first synchronizes to the BS using the SCH. It then tries to decode the data in the BCH. If the BCH can be decoded successfully, i.e., the cyclic redundancy check (CRC) is positive, then the channel estimation procedure is started. The channel estimation procedure consists of two steps. Firstly, the pilot symbols are derotated with respect to the first pilot symbol to reduce the phase-shift noise generated by the dual-RF CardBus/PCMCIA card. Secondly, the pilot symbols are averaged to increase the measurement SNR. The estimated MIMO channel is finally stored to disk. For a more detailed description of the synchronization and channel estimation procedure see [10, 11].

4.2. Measurements

The measurements were conducted outdoors in the vicinity of Eurecom in Sophia Antipolis, France[4]. The scenario is characterized by a semi-urban hilly terrain, composed by short buildings and vegetation with a predominantly present LOS. Fig. 4 shows a map of the environment. The BS is located at the roof of Eurecom's southmost building. The antenna is directed towards Garbejaire, a small nearby village. The measurement parameters are summarized in Table 1.

In this paper we use two different sets of measurements. In measurement 1, the UE was placed inside a standard passenger car which was being driven with an average speed of 50km/h along the routes shown in Fig. 4. The channel conditions are changing between line of sight (LOS) and non-LOS (NLOS). In measurement 2, the UE is more or less stationary on the parking lot in the bottom right corner of Fig. 4. This scenario is LOS.

5. REAL CHANNEL PERFORMANCE

In the simulations, we consider the particular real channel measured as commented in section 4 with 4 transmit and 2 receive antennas. Note that for the evaluations in this paper we have selected only one subcarrier to mimic a narrowband system. We show results for three cases: perfect CSI at the transmitter, non-differential Grassmannian packaging [4], and differential quantization of the channel correlation matrices $\mathbf{R}_H(n)$ using geodesic curves [3]. In all the cases, simulations were performed using the optimum strategies to maximize the mutual information and the SNR. The strategy that maximizes the mutual information corresponds to a waterfilling distribution of power over the eigenmodes of the channel, and the strategy that maximizes the SNR uses only the strongest eigenmode of the available channel response.

We considered two cases for the feedback. In the first case the quantized CSI is transmitted instantaneously from the receiver to the transmitter. That is, the transmitter had knowledge of the quantized version of the current channel matrix. In a real situation, however, the transmission delay through the feedback channel is not zero and this affects the performance of the system. Therefore we also studied the case where we introduce delay in the feedback channel.

5.1. Feedback with no delay

As shown in Fig. 5, the differential strategy exploits the time-correlation of the channel and converges to perfect CSIT case, while the performance using the non-differential quantization is lower, even when using more feedback bits. Also note that the differential quantization works better in more slow-varying channels and worse in the scenarios of high mobility

[4]Eurecom has a frequency allocation for experimentation around its premises.

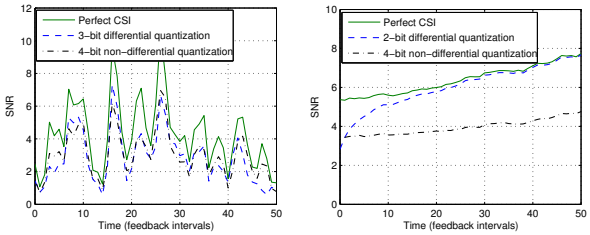

(a) SNR in a high mobility scenario (measurement 1)
(b) SNR in a low mobility scenario (measurement 2)
(c) MI in a high mobility scenario (measurement 1)
(d) MI in a low mobility scenario (measurement 2)

Fig. 5. Different feedback techniques in realistic channels.

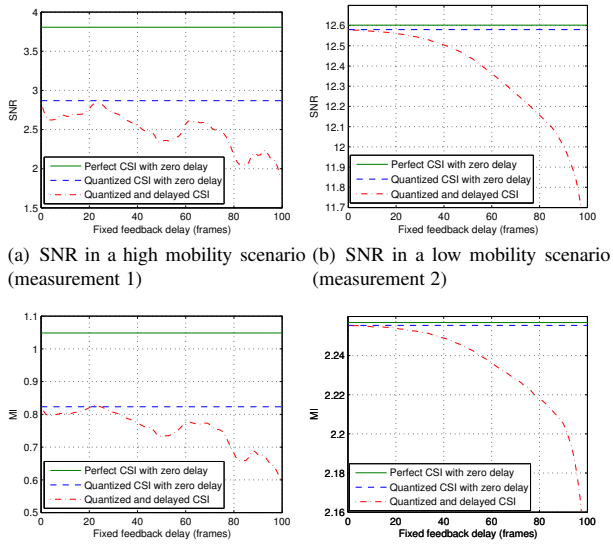

(a) SNR in a high mobility scenario (measurement 1)
(b) SNR in a low mobility scenario (measurement 2)
(c) MI in a high mobility scenario (measurement 1)
(d) MI in a low mobility scenario (measurement 2)

Fig. 6. Effects of feedback delay in realistic channels.

where the channel is fast-fading.

5.2. Delay in the feedback channel

The simulations corresponding to Fig. 6 analyze the impact of the feedback delay on the performance of the system. The plot shows the averaged SNR and mutual information (MI) for the high mobility and low mobility scenarios described in section 4 versus the delay measured in frames (e.g., a delay equal to 10 means that the delay is equal to 10 frames). For the simulations a window containing frames from 500 to 520 was used to calculate the average SNR and mutual information. Three situations are compared: perfect CSI at the transmitter, differential feedback with no delay, and differential feedback with different values for the delay in the feedback link. The main conclusion is that the performance rapidly decreases when the delay exceeds a threshold.

6. CHANNEL PREDICTION

In order to reduce or compensate the effect of feedback delay, channel prediction strategies can be used. If the receiver can predict the behavior of the channel response matrix and knows the value of the delay in the feedback channel, it is possible to send through the feedback link a quantized version of the prediction of the CSI. This way, the transmitter will receive the prediction of the current channel instead of the delayed CSI.

6.1. Algorithm description

The algorithm described in this section predicts each component of the channel response matrix $\mathbf{H}(n)$ separately using a Wiener predictor; this means that $n_R n_T$ predictors will be used. The objective of the Wiener predictor [12] is to minimize the quadratic error. The N predictor coefficients $\mathbf{g}_{ij}$ for the $_{ij}$ component of $\mathbf{H}(n)$ are defined as:

$$\mathbf{g}_{ij} = \arg\min_{\mathbf{g}_{ij}} \mathbb{E}[|e_{ij}(n)|^2] \in \mathbb{C}^N. \tag{10}$$

For a filter order N, and a prediction of L delay intervals, the error at time instant n is defined as

$$e_{ij}(n) = x_{ij}(n+L) - \mathbf{g}_{ij}^H \mathbf{x}_{ij}(n), \tag{11}$$

where the vector of samples $\mathbf{x}_{ij}(n)$ is

$$\mathbf{x}_{ij}(n) = \begin{bmatrix} x_{ij}(n) \\ x_{ij}(n-1) \\ \vdots \\ x_{ij}(n-N) \end{bmatrix} \in \mathbb{C}^N \text{and} \quad x_{ij}(n) = [\mathbf{H}(n)]_{ij}.$$

Then the quadratic error can be written as

$$\begin{aligned} |e_{ij}(n)|^2 =& \mathbf{g}_{ij}^H \mathbf{x}_{ij}(n) \mathbf{x}_{ij}^H(n) \mathbf{g}_{ij} + |x_{ij}(n+L)|^2 \\ & - \mathbf{g}_{ij}^H \mathbf{x}_{ij}(n) x_{ij}^*(n+L) - \mathbf{x}_{ij}^H(n) \mathbf{g}_{ij} x_{ij}(n+L). \end{aligned} \tag{12}$$

The predictor vector $\mathbf{g}_{ij}$ that minimizes the average of expression (12) can be easily proven to be [12]:

$$\mathbf{g}_{ij} = \left(\sum \mathbf{x}_{ij}(n)\mathbf{x}_{ij}^H(n)\right)^{-1}\left(\sum \mathbf{x}_{ij}(n)x_{ij}^*(n+L)\right), \quad (13)$$

where the sum is applied to the set of data that is available for the calculation of the predictor. This way, it is possible to predict the CSI with a delay of L time instants and design the transmitter based on the quantized version of the predicted CSI.

6.2. Simulations in real channel

The impact of channel prediction to compensate for the feedback delay will be analyzed in this section, using the realistic channel measured with EMOS. The same realistic channel studied in section 5 is used for this analysis. The simulations corresponding to Fig. 7 show the impact of prediction in a system with feedback delay. The plot shows the averaged SNR and mutual information for the high mobility and low mobility scenarios versus the delay measured in frames. For the simulations a window containing frames from 500 to 520 was used to calculate the average SNR and mutual information. Three situations are compared: perfect CSI at the transmitter, differential feedback with no delay, and differential feedback with different values for the delay in the feedback link using a Wiener predictor of order 10.

It can be seen from Fig. 7 that there is no substantial improvement when compared to the simulations without prediction from section 5.2. It would be interesting to observe the performance of the predictor in a channel that can be predicted more accurately, for example a channel that follows an autoregressive (AR) model. This case will be studied in the following section.

6.3. Simulations in an AR channel

The predictor will now be tested on a synthetic channel generated using an autoregressive (AR) model of order Q. An AR model is described by the following equation [13]:

$$\mathbf{H}(n) = \sum_{q=1}^{Q} a_q \mathbf{H}(n-q) + \mathbf{W}(n), \quad (14)$$

where a_q are the autoregressive coefficients and the components of matrix $\mathbf{W}(n)$ are Gaussian, independent and with variance such that $\mathbb{E}\left[|[\mathbf{H}(n)]_{ij}|^2\right] = 1$.

Note that the predictor equals the coefficients of the AR model if the delay is 1 frame, but this is no longer the case for larger delays. In this last situation the coefficients should be computed as described in section 6.1.

In Fig. 8 we show the results of the differential feedback scheme applied to a channel generated using an AR model of order 10 with following AR coefficients: $a_1 = 1.4351 + 2.8308i$, $a_2 = 1.7196 - 2.9843i$, $a_3 = -0.9942 + 0.4452i$, $a_4 = -0.3001 - 0.6810i$, $a_5 = 0.1308 + 0.3598i$, $a_6 = -0.4145 + 0.0475i$, $a_7 = 0.1692 - 0.0565i$, $a_8 = -0.0661 + 0.3097i$, $a_9 = 0.1428 - 0.1975i$ and $a_{10} = -0.0702 + 0.0268i$. The simulations show that the predictor works best up to a delay of 10 frames, which corresponds to the order of the AR model. After that point, the gain decreases slowly.

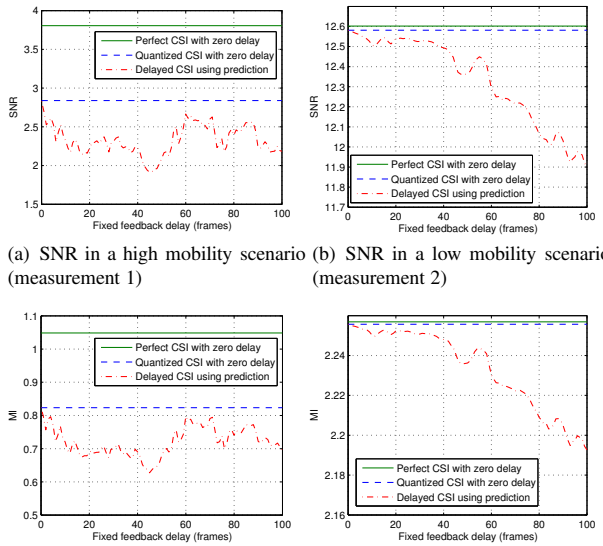

(a) SNR in a high mobility scenario (measurement 1)
(b) SNR in a low mobility scenario (measurement 2)
(c) MI in a high mobility scenario (measurement 1)
(d) MI in a low mobility scenario (measurement 2)

Fig. 7. CSI prediction used to reduce the effect of feedback delay in realistic channels.

7. CONCLUSIONS

This paper has presented an evaluation of differential and non-differential feedback strategies in realistic MIMO systems. The main objective has been the study of the impact of such techniques using real channel measurements performed with the EMOS for high and low mobility scenarios and under different situations of delay in the feedback link.

The differential feedback strategy performed much better than the non-differential strategies like Grassmannian packaging in low mobility channels, while in high mobility channels the performance was similar. Simulations using realistic channel data showed that a delay in the feedback channel affects specially high mobility channels because they vary faster. For small amounts of delay (less than 20 frames) the performance loss was around 10% in high mobility channels and less in the slow-varying cases.

The proposed technique to reduce the effect of feedback delay based on channel prediction performed well using a synthetic channel model. However, it was not able to compensate the delay in the measured channels. This showed that

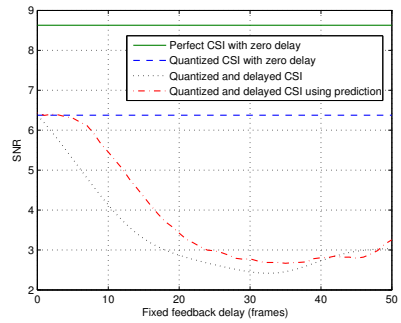

(a) SNR performance

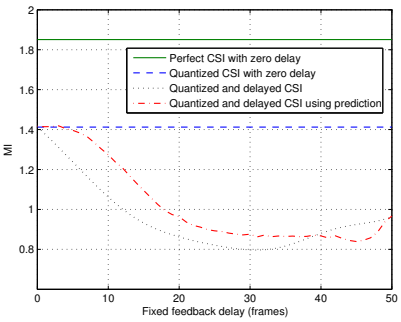

(b) Mutual Information performance

Fig. 8. CSI prediction used to reduce the effect of feedback delay in an AR(10) channel.

channel models are often too simplistic and do not provide realistic performance results.

8. REFERENCES

[1] J. Yang and D. Williams, "Transmission Subspace Tracking for MIMO Systems With Low-Rate Feedback," *IEEE Trans. on Communications*, vol. 55, no. 8, pp. 1629–1639, Aug. 2007.

[2] M. Talih, "Geodesic Markov Chains on Covariance Matrices," Statistical and Applied Mathematical Sciences Institute, Tech. Rep., March 2007. [Online]. Available: http://www.samsi.info/TR/tr2007-04.pdf

[3] D. Sacristán-Murga and A. Pascual-Iserte, "Differential Feedback of MIMO Correlation Matrices based on Geodesic Curves," in *Proc. IEEE International Conference on Acoustics, Speech and Signal Processing (ICASSP 2009)*, Taipei, Taiwan, April 2009, accepted.

[4] D. Love, R. Heath, and T. Strohmer, "Grassmannian Beamforming for Multiple-Input Multiple-Output Wireless Systems," *IEEE Trans. on Information Theory*, vol. 49, no. 10, pp. 2735–2747, Oct. 2003.

[5] F. Kaltenberger, M. Kountouris, D. Gesbert, and R. Knopp, "Correlation and Capacity of Measured Multi-user MIMO Channels," in *Proc. IEEE Intl. Symp. on Personal, Indoor and Mobile Radio Comm. (PIMRC)*, Cannes, France, Sept. 2008.

[6] ——, "Performance of Multi-user MIMO Precoding with Limited Feedback over Measured Channels," in *Proc. IEEE Global Communications Conference (IEEE GLOBECOM 2008)*, New Orleans, USA, Nov.–Dec. 2008.

[7] D. Palomar, J. Cioffi, and M. Lagunas Hernández, "Joint Tx-Rx Beamforming Design for Multicarrier MIMO Channels: a Unified Framework for Convex Optimization," *IEEE Trans. on Signal Processing*, vol. 51, no. 9, pp. 2381–2401, Sept. 2003.

[8] S. Boyd and L. Vandenberghe, *Convex Optimization*. Cambridge University Press, 2004.

[9] G. Golub and C. Van Loan, *Matrix Computations*. The Johns Hopkins University Press, Oct. 1996.

[10] R. de Lacerda, L. S. Cardoso, R. Knopp, M. Debbah, and D. Gesbert, "EMOS platform: real-time capacity estimation of MIMO channels in the UMTS-TDD band," in *Proc. International Symposium on Wireless Communication Systems (IWCS)*, Trondheim, Norway, Oct. 2007.

[11] F. Kaltenberger, L. Bernardo, and T. Zemen, "Characterization of measured multi-user mimo channels using the spectral divergence measure," COST 2100, Lille, France, Tech. Rep. TD(08) 640, Nov. 2008.

[12] N. Wiener, *The extrapolation, interpolation and smoothing of stationary time series with engineering applications*. Wiley, 1949.

[13] P. Stoica and R. L. Moses, *Introduction to Spectral Analysis*. Prentice Hall, 1997.